

Terahertz bound states in the continuum on-and-off- Γ point of a moiré photonic superlattice

XUELIAN ZHANG,^{1,†} ZHENYU ZHAO,^{1,†,*} PEILIANG LIU,¹ RAJOUR TANYI AKO,² SHARATH SRIRAM,² XUAN ZHAO,³ HONGXIN LIU,³ AND HAIJUN BU^{3,4}

¹Department of Physics, Shanghai Normal University, Shanghai 200234, China

²Functional Materials and Microsystems Research Group and the Micro Nano Research Facility, ARC Centre of Excellence for Transformative Meta-Optical Systems, RMIT University, Melbourne, VIC, 3000, Australia

³Suzhou Institute of Metrology, Suzhou 215163, China

⁴buhj@szjl.com.cn

[†]These authors contributed equally to this Letter.

*zyzhao@shnu.edu.cn

Received 5 September 2024; revised 23 October 2024; accepted 7 November 2024; posted 11 November 2024; published 6 December 2024

Moiré metasurfaces exhibit high optical tuneabilities and versatile light manipulation capabilities. Both infinite quality factor (Q factor) and topological vortex configurations in momentum space (k -space) of the bound state in the continuum (BIC) have introduced new dimensions for light modulation. Herein, we propose a moiré metasurface comprising two identical square photonic lattices superimposed with a commensurate angle of 12.68° . By tuning the incidence angle, the symmetric-protected BICs, Friedrich–Wintgen BIC, and accidental BIC can be achieved simultaneously in our moiré metasurfaces. It is found that the quasi-BICs maintain an ultrahigh Q factor beyond 10^7 . The photonic band structures manifest that the three types of BICs are at the center of far-field polarization vortices in k -space, which have their own topological charges. We experimentally show that these BICs exhibit high sensitivity to subtle changes in analyte refractive index for thin-film sensor application. Our discovery predicts an approach to a highly sensitive multi-channel terahertz biosensor. © 2024 Optica Publishing Group. All rights, including for text and data mining (TDM), Artificial Intelligence (AI) training, and similar technologies, are reserved.

<https://doi.org/10.1364/OL.541438>

Moiré metasurfaces can be created by the interference of two or more periodic fringes with relative differences in lattice constants or commensurate angles. This approach is employed to precisely and easily manipulate the interacting photons [1,2]. Owing to the moiré photonic superlattice layout, such metasurfaces exhibit photonic flatband, chirality conversion, and vortex tenability [3,4]. Compared to the tedious manipulations of individual meta-atoms and complex spatial arrangements, moiré metasurfaces can achieve a large-scale functional area of a photonic device with highly optical tenability by tuning the twisted angles between individual photonic lattices. Therefore, moiré metasurfaces have more abundant photonic responses than their periodic counterparts owing to the quasi-periodicity of the moiré fringes [5,6]. These properties open up a wide range of possibilities for the exploration of entirely new physical

phenomena and device architectures. Furthermore, the distinguished BIC by considering two types of polarizations has been proposed in the one-dimensional superlattice [7]. Additionally, such metasurfaces possess untapped topological characteristics and infinite Q factors, meaning infinite photonic lifetime on the state. Particularly, in quasi-periodic structures with well-defined wave vectors, the bound states in the continuum (BICs) exhibit far-field topological charges in momentum space. These unique properties led to numerous applications in lasers [8,9] and sensors [10,11]. With these advantages, the generation and manipulation of BICs in the first Brillouin zone (FBZ) of an artificial moiré photonic superlattice at very low energy level of meV has not been properly investigated.

Herein, we propose a terahertz moiré metasurface that exhibits the symmetric-protected BICs (SP-BICs), Friedrich–Wintgen BIC (FW-BIC), and accidental BIC relying on the incident terahertz mode of TE and TM polarization, respectively. Our moiré metasurface is constructed by superimposing two initial square photonic lattices with a commensurate angle of 2α , where the first layer of the square photonic lattices is twisted counterclockwise by an angle, α , and the second layer is twisted clockwise by an angle, α . The distance between two layers is zero. The meta-atoms on the site of the square photonic lattices are metallic disks made up of perfect electric conductor (PEC). However, most of the metals exhibit a PEC behavior at the terahertz band.

Regarding the quasi-BICs that occurred in the twisted bilayer graphene of the hexagonal lattice close to 10° [6], we hereby select a specific commensurate angle of $2\alpha = 12.68^\circ$ at which the moiré metasurface forms a quasi-periodic photonic superlattice with translational symmetry. The schematic diagram is illustrated in Fig. 1(a). The radius of the disk, r , is $6\mu\text{m}$, and the spacing between two adjacent disks is $8\mu\text{m}$, resulting in a square photonic lattice period, p , of $20\mu\text{m}$. The thickness of all disks is $0.2\mu\text{m}$. Correspondingly, the calculated quasi-periodicity of the moiré photonic superlattice, L_m , is $128.06\mu\text{m}$ [12]. The size of the proposed metasurface is 1cm^2 . Figure 1(b) shows the schematic diagram of the moiré metasurface excited obliquely by planar terahertz waves. The terahertz transmittance

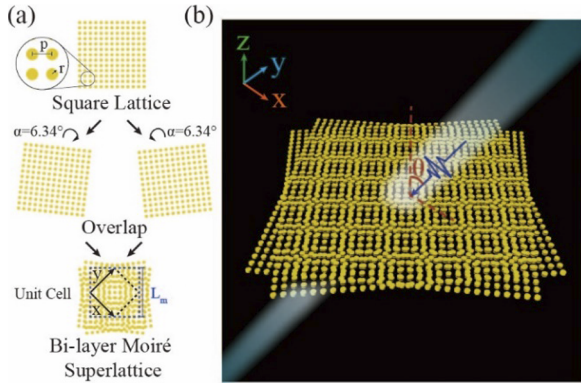


Fig. 1. (a) Schematic of the initial square photonic lattice and the corresponding moiré fringes. The circular dots indicate the disks of PEC. α denotes the twisting angle, and the dashed area marks the unit cell. (b) Schematic diagram shows a terahertz pulse obliquely incident on the proposed moiré metasurface.

of the moiré metasurface was simulated by using the frequency-domain solver of the CST Microwave Studio platform. Periodic boundary conditions were applied along the x and y directions, while perfectly matching layers were applied along the z direction. The mesh is set to adaptive mode. The incident terahertz pulse is parallel to the xy -plane at an angle θ relative to the z axis. Here, the in-plane terahertz polarization is in the transverse electric mode (TE mode), while the out-of-plane polarization is in the transverse magnetic mode (TM mode). The photonic band structure is obtained by using the eigenfrequency solver in COMSOL Multiphysics [13]. The permittivity of polyimide, ϵ , is 3.5, with the thickness of 75 μm .

The transmittance of the proposed moiré metasurface versus the oblique incidence angle of terahertz waves and the Q factor trajectories of different types of quasi-BIC as a function of oblique incidence angle are presented in Fig. 2. In the case of the TM mode excitation, the ν_1 and ν_2 resonance modes exhibit anti-crossing behavior as the incidence angle θ increases. The ν_1 and ν_2 resonance modes at 1.45 THz vanishes at an incidence angle of $\theta = 15.4^\circ$, marked by a white circle in Fig. 2(a). As θ deviates from 15.4° , a transmission dip gradually appears in the transmittance spectrum. Here, we consider the general scenario where the two resonances have different frequencies ν_1 and ν_2 with different radiation rates γ_1 and γ_2 . The two resonances radiate into the same channel, so interference of terahertz radiation gives rise to the coupling term. The effective non-Hermitian Hamiltonian can be written as follows [14]:

$$H = \begin{pmatrix} \nu_1 & \kappa \\ \kappa & \nu_2 \end{pmatrix} + i \begin{pmatrix} \gamma_1 & \pm\sqrt{\gamma_1\gamma_2} \\ \pm\sqrt{\gamma_1\gamma_2} & \gamma_2 \end{pmatrix}, \quad (1)$$

where ν_1 and ν_2 are the resonant frequencies of two modes, γ_1 and γ_2 are the decay rates, and κ and $\pm(\gamma_1\gamma_2)^{-1/2}$ are the near-field coupling and the far-field interference coefficients, respectively. BIC is reported to emerge when these parameters satisfy the Friedrich–Wintgen condition:

$$\kappa(\gamma_1 - \gamma_2) = \pm\sqrt{\gamma_1\gamma_2}(\nu_1 - \nu_2). \quad (2)$$

When $\kappa \approx 0$ or $\gamma_1 \approx \gamma_2$, Friedrich–Wintgen BICs occur near the frequency crossings of the uncoupled resonances. In our case, at an incidence angle, $\theta = 15.4^\circ$, the Friedrich–Wintgen condition is satisfied since the decay rate of one mode vanishes,

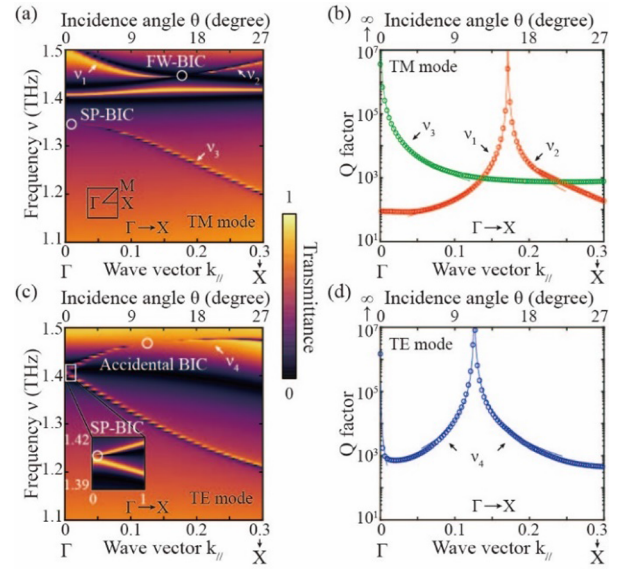


Fig. 2. (a) Transmittance of the proposed moiré metasurface as a function of frequency and incidence angle in the TM mode excitation. The inset represents the diagram of the first Brillouin zone. (b) Q factor trajectories of the FW-quasi-BIC and SP-quasi-BIC in the TM mode excitation. Red curve: Q factor trajectories of the ν_1 and ν_2 resonance modes. Green curve: Q factor trajectories of the ν_3 resonance mode. (c) Transmittance of the proposed moiré metasurface as a function of frequency and incidence angle in the TE mode excitation. (d) Q factor trajectories of the SP-quasi-BIC and accidental quasi-BIC in the TE mode excitation. Blue curve: Q factor trajectories of the ν_4 resonance mode.

effectively forming a bound state, while the other mode retains a higher decay rate. In other words, a destructive interference occurs between distinct modes when the FW-BIC emerges at $\theta = 15.4^\circ$. Furthermore, the degrading ratio of the radiative Q factor of the ν_1 resonance mode as a function of incidence angle, shown in Fig. 2(b), exhibits asymmetric behavior off the Γ point, which is the significant evidence of the FW-BIC [15].

Additionally, the ν_3 resonance mode redshifts from 1.34 THz to 1.18 THz with the incidence angle tilting gradually from 0° to 30° . The ν_3 resonance mode at 1.34 THz vanishes at an incidence angle of $\theta = 0^\circ$, marked by a white circle in Fig. 2(a). At $\theta = 0^\circ$, the moiré metasurface exhibits a reflection symmetry as well as a rotational symmetry owing to the C_4 structural symmetry of the square lattice, modes of the aforementioned symmetry classes that completely decouple lead a bound state of one symmetry class embedded in the continuous spectrum of modes of another symmetry class, and the coupling is forbidden owing to the symmetry preservation of the C_4 structure. Regarding the quasi-periodicity in the xy -plane, the 0° rotational symmetry around the z axis (C_4) is preserved, commonly known as the Γ point in k -space. The SP-BIC at the Γ point can also be considered as a result of the coupling of the degenerated modes of the aforementioned symmetry classes [16]. Meanwhile, the radiative Q factor of the ν_3 resonance mode is satisfied with the inverse square formula of the asymmetry parameter $a(\theta)$ ($Q \propto a(\theta)^{-2}$), as shown in Fig. 2(b). As such, the vanished point at 1.34 THz is approved to be a SP-BIC [17].

In the case of the TE mode excitation, the ν_4 resonance mode is blueshifted from 1.41 THz to 1.48 THz with increasing angle of incidence, as shown in Fig. 2(c). The ν_4 resonance mode at

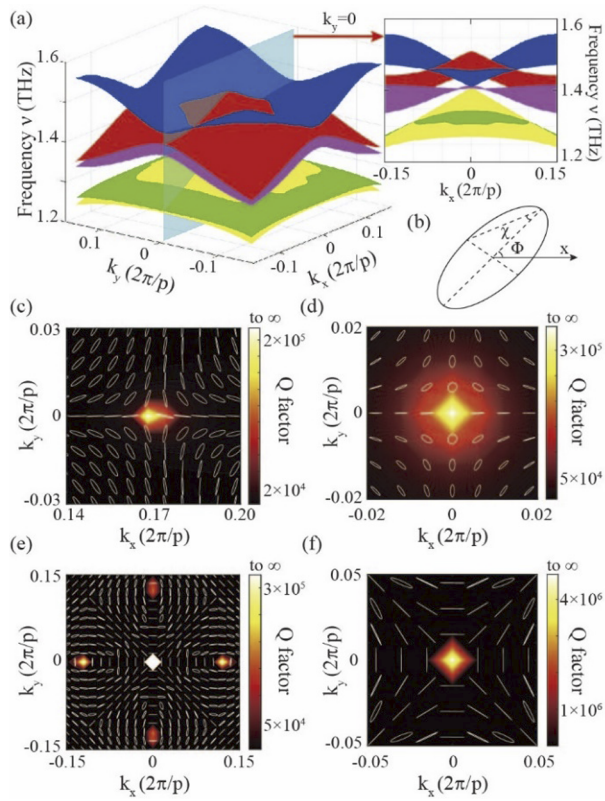


Fig. 3. (a) Three-dimensional representations of the topological band structure around the Γ point. (b) Schematic of a single polarization vector. Φ : the orientation angle reflecting the amplitude-proportional relationship between the electric field components along the x (E_x) and y (E_y) directions. χ : the inverse tangent ellipticity reflecting the absolute phase difference between E_x and E_y components. (c)–(f) Calculated polarization vectors around the BICs with Q factors as the background in the first Brillouin zone in both TM and TE mode excitation, respectively.

1.41 THz vanishes at an incidence angle of $\theta = 0^\circ$, indicated on Fig. 2(c) by a white circle. Similar to the ν_3 resonance mode, the vanished point at 1.41 THz is a SP-BIC, and the correspondingly radiative Q factor of the ν_4 resonance mode at the Γ point satisfies the inverse square formula, shown in Fig. 2(d). Interestingly, the transmittance spectra of the ν_4 resonance mode at 1.47 THz accidentally vanish at an incidence angle of $\theta = 11.3^\circ$, marked on Fig. 2(c) with white circles. The transmittance spectrum of the metasurface at an incidence angle of $\theta = 11.3^\circ$ exhibits an asymmetric Fano line shape, indicating that the radiating source weakly interacts with the free space, thereby significantly reducing the radiative loss in the moiré metasurface. Owing to the accidental cancellation of radiation, an accidental BIC is arising. As shown in Fig. 2(d), the Q factor first exponentially increases and then exponentially decreases along with a maximal point that depicts the ideal accidental BIC with infinite Q factor. So, the vanished point at 1.47 THz is demonstrated to be an accidental BIC. Such an accidental BIC is similar to the dielectric metasurface excited by the TM mode radiation [18,19].

BICs are identified as topological defects in momentum space, and the topological charge they carry is defined by the winding major axis of the polarized states around the BICs [20,21]. The momentum space of the moiré photonic superlattice excited by

the TE and TM mode terahertz radiation reveals intrinsic topological properties of all different BICs, as shown in Figs. 3(a) and 3(b). They illustrate the topological band structure around the Γ point and polarization ellipses formed by electric field vectors. The topological charges can be defined as follows [20,22]:

$$q = \frac{1}{2\pi} \oint_c dk \cdot \nabla_k \phi(\mathbf{k}), \quad (3)$$

where $\Phi(\mathbf{k})$ is the angle between the polarization major axis and the x axis and c is a closed path in the k -space around the BICs along the anticlockwise direction. The topological charge can be identified by counting the winding numbers of polarization vectors in an anticlockwise direction. The far-field polarization of the ν_1 , ν_3 , and ν_4 resonance modes are calculated within the first Brillouin zone (FBZ) where BICs occur, as shown in Figs. 3(c)–3(e). Figure 3(f) represents the enlarged image of the central region near the Γ point in Fig. 3(e). Notably, the far-field polarization directions exhibit winding around BICs where the Q factor approaches infinity, forming polarization vortices. In the TM mode excitation, both the FW-BIC and SP-BIC are topologically protected by an identical topological charge of -1 . In the TE mode excitation, the SP-BIC at the Γ point is topologically protected by a charge of -1 , while the accidental BIC at the off- Γ point is also topologically protected but carries an opposite charge of $+1$, which coexisted at the ν_4 resonance mode. These topological properties provide another strong evidence for the existence of BICs [20].

To demonstrate the sensitivity of the abovementioned fabricated moiré metasurface, their performance is evaluated with the help of a $10\ \mu\text{m}$ thick artificial analyte thin film with different refractive indices (n). The simulated resulting transmission resonance is shown in Fig. 2, when incident obliquely with terahertz waves at a fixed incidence angle $\theta = 22.0^\circ$. The chosen angle of incidence produces sharp resonance of the SP-quasi-BIC, FW-quasi-BIC, and accidental quasi-BIC, respectively. Here, n varies from 1.0 to 1.5 with a step size of 0.1. The frequency shift of the above sharp resonance is shown in Figs. 4(a) and 4(b). When n increases, the quasi-BIC is redshifted. Sensitivity (S) is defined as $S = \Delta\nu / \Delta n$ in which Δn represents the difference in refractive index between the analytes, as shown in Figs. 4(c) and 4(d). The frequency shift of all the quasi-BICs correlates well with Δn . Although the conductivity of a metal and the loss tangent of polyimide are both having a significant impact on the Q factor of the quasi-BICs, the quasi-BICs still exhibit high Q factors in practical applications [23,24]. Additionally, the integration of micro-electromechanical system technology with metasurfaces holds promising potential for achieving tunable optical properties [25].

Table 1 lists the sensitivity of the aforementioned quasi-BIC in GHz per refractive index unit (GHz/RIU). All the quasi-BIC shift at 11 ± 0.5 GHz with n increases by 0.1.

In conclusion, we propose a moiré photonic superlattice composed of two identical square photonic lattices superimposed with a commensurate angle of 12.68° . Our investigations show that our proposed design supports the SP-BIC, FW-BIC, and accidental BIC on-and-off the Γ points when incident with the terahertz mode of TE and TM polarization, respectively. The evolution from ideal BICs to quasi-BICs can be induced by tuning the incidence angle θ . It is found that the quasi-BICs maintain an ultrahigh Q factor beyond 10^7 . The temporal coupled-mode theory is employed to reveal the underlying physics of the FW-BIC. The topological band structures manifest that the FW-BIC

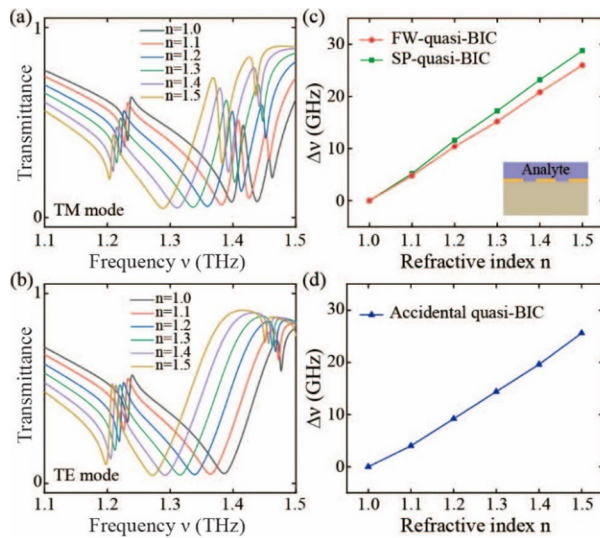


Fig. 4. (a) and (b) Transmittance spectra of the moiré metasurface sensor with analyte for different refractive indices in both TM and TE mode excitation, respectively. (c) and (d) Simulated sensitivity analysis of the sensing model at different quasi-BICs for different refractive indices.

Table 1. Sensitivity Analysis of the Proposed Moiré Metasurface for Analytes of Different n

n	Sensitivity (GHz/RIU)		
	FW-Quasi-BIC	SP-Quasi-BIC	Accidental Quasi-BIC
1.1	9.6	10.4	8.0
1.2	20.8	23.2	18.4
1.3	30.4	34.4	28.8
1.4	41.6	46.4	39.2
1.5	52.0	57.6	51.2

and SP-BIC are at the center of far-field polarization vortices in k -space, which are both topologically protected with a charge of -1 in the TM mode excitation. Interestingly, the SP-BIC at the Γ point is topologically protected by a charge of -1 , while the accidental BIC at the off- Γ point is also topologically protected but carries an opposite charge of $+1$. This occurs at the ν_4 resonance mode in the TM mode excitation. The biosensing performance of the aforementioned quasi-BICs are evaluated by introducing a 10 μm thin film of analytes with different refractive

indices ranging from 1.0 to 1.5, and all the quasi-BIC exhibit 11 ± 0.5 GHz/RIU. Our findings manifest a novel approach to achieve multiple terahertz BICs with high tunability for medical biosensor application.

Funding. Science and Technology Program of Jiangsu Administration for Market Regulation (KJ2024021); National Natural Science Foundation of China (62475159).

Acknowledgment. This work was performed in part at the Micro Nano Research Facility at RMIT University in the Victorian Node of the Australian National Fabrication Facility (ANFF).

Disclosures. The authors declare no conflicts of interest.

Data availability. Data underlying the results presented in this paper are not publicly available at this time but may be obtained from the authors upon reasonable request.

REFERENCES

- S. Zhao, R. Kitaura, P. Moon, *et al.*, *Adv. Sci.* **9**, 2103460 (2022).
- P. Wang, Y. Zheng, X. Chen, *et al.*, *Nature* **577**, 42 (2020).
- B. Lou, N. Zhao, M. Minkov, *et al.*, *Phys. Rev. Lett.* **126**, 136101 (2021).
- T. Zhang, K. Dong, J. Li, *et al.*, *Nat. Commun.* **14**, 6014 (2023).
- C. Ma, S. Yuan, P. Cheung, *et al.*, *Nature* **604**, 266 (2022).
- L. Huang, W. Zhang, and X. Zhang, *Phys. Rev. Lett.* **128**, 253901 (2022).
- S. Hu, Z. Guo, W. Liu, *et al.*, *Nat. Commun.* **15**, 2773 (2024).
- Y. Ren, P. Li, Z. Liu, *et al.*, *Sci. Adv.* **8**, eade8817 (2022).
- C. Huang, C. Zhang, S. Xiao, *et al.*, *Science* **367**, 1018 (2020).
- M. Meudt, C. Bogiadzi, K. Wrobel, *et al.*, *Adv. Opt. Mater.* **8**, 2000898 (2020).
- Y. Chen, C. Zhao, Y. Zhang, *et al.*, *Nano Lett.* **20**, 8696 (2020).
- J.-H. Han, I. Kim, J.-W. Ryu, *et al.*, *Opt. Express* **23**, 17443 (2015).
- M. Kang, L. Mao, S. Zhang, *et al.*, *Light: Sci. Appl.* **11**, 228 (2022).
- W. Suh, Z. Wang, and S. Fan, *IEEE J. Quantum Electron.* **40**, 1511 (2004).
- P. Liu, Z. Zhao, Y. Xue, *et al.*, *Opt. Lett.* **49**, 1301 (2024).
- P. Hu, J. Wang, Q. Jiang, *et al.*, *Optica* **9**, 1353 (2022).
- K. Koshelev, S. Lepeshov, M. Liu, *et al.*, *Phys. Rev. Lett.* **121**, 193903 (2018).
- C. W. Hsu, B. Zhen, J. Lee, *et al.*, *Nature* **499**, 188 (2013).
- Q.-K. Liu, X.-Q. Luo, X. Xu, *et al.*, *Phys. Rev. B* **107**, 205422 (2023).
- B. Zhen, C. W. Hsu, L. Lu, *et al.*, *Phys. Rev. Lett.* **113**, 257401 (2014).
- Y. Zhang, A. Chen, W. Liu, *et al.*, *Phys. Rev. Lett.* **120**, 186103 (2018).
- H. Tong, S. Liu, M. Zhao, *et al.*, *Nat. Commun.* **11**, 5216 (2020).
- G. Sun, Y. Wang, Z. Cui, *et al.*, *Appl. Phys. Lett.* **124**, 111704 (2024).
- X. Zhao, C. Chen, K. Kaj, *et al.*, *Optica* **7**, 1548 (2020).
- X. Wang, C. Huang, Z. Sun, *et al.*, *ACS Photonics* **11**, 3870 (2024).